THE JOURNAL OF PHYSICAL CHEMISTRY B

Article

pubs.acs.org/JPCB

Loop-Closure and Gaussian Models of Collective Structural Characteristics of Capped PEO Oligomers in Water

M. I. Chaudhari and L. R. Pratt*

Department of Chemical and Biomolecular Engineering, Tulane University, New Orleans, Louisiana 70118, United States

M. E. Paulaitis

Department of Chemical and Biomolecular Engineering, The Ohio State University, Columbus, Ohio 43210, United States

ABSTRACT: Parallel-tempering MD results for a $CH_3(CH_2{-}O{-}CH_2)_mCH_3$ chain in water are exploited as a database for analysis of collective structural characteristics of the PEO globule with a goal of defining models permitting statistical thermodynamic analysis of dispersants of Corexit type. The chain structure factor, relevant to neutron scattering from a deuterated chain in null water, is considered specifically. The traditional continuum-Gaussian structure factor is inconsistent with the simple $k \to \infty$ behavior, but we consider a discrete-Gaussian model that does achieve that consistency. Shifting and scaling the discrete-Gaussian model helps to identify the low-k to high-k transition near $k \approx 2\pi/0.6$ nm when an empirically matched number of Gaussian links is about one-third of the total number of effective atom sites. This short distance-scale boundary of 0.6 nm is directly verified with the r space distributions, and this distance is thus identified with a natural size for coarsened monomers. The probability distribution of R_g^2 is compared with the classic predictions for both the Gaussian model and freely jointed chains. $\langle R_g^2(j)\rangle$, the contribution of the jth chain segment to $\langle R_g^2\rangle$, depends on the contour index about as expected for Gaussian chains despite significant quantitative discrepancies that express the swelling of these chains in water. Monomers central to the chain contour occupy the center of the chain globule. The density profiles of chain segments relative to their center of mass can show distinctive density structuring for smaller chains due to the close proximity of central elements to the globule center. However, that density structuring washes out for longer chains where many chain elements additively contribute to the density profiles. Gaussian chain models thus become more satisfactory for the density profiles for longer chains.

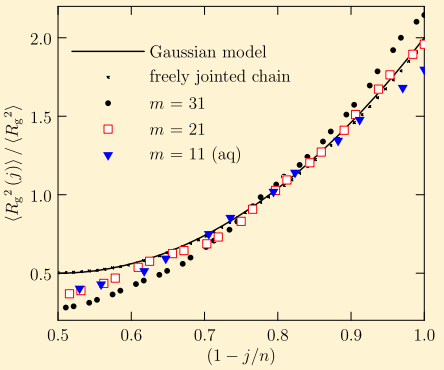

1. INTRODUCTION

Arguably the most important water-soluble synthetic polymers,[1,2] $(-CH_2-O-CH_2-)_n$ chain molecules are intrinsic to the dispersant materials applied to oil spills[3] and can be soluble also in organic solvents. With −H (and thus methyl $-CH_3$) ends, poly(ethylene oxide) (PEO) is a common name, and we will use that name generically when the chains have arbitrary capping groups. With hydroxyl −OH terminations, these chains are typically called polyethylene glycol (PEG), and we will use that name in discussing experiments that study that case specifically.

For dispersants used on oil spills[3] and for other applications,[4] PEO chains are often decorated with junctions or tails or caps. Correlations associated with capping groups then focus molecular structural analyses, molecular specificity in understanding loop closure being an outstanding interest.[5] Those correlations can be the targets of neutron scattering experiments[6] with deuterated chains, under the important limitation of chemical feasibility of specific isotopic labeling of the caps. We have studied $X(-CH_2-O-CH_2-)_nX$ with a variety of capping groups X for just those reasons.[7] Capping groups can nontrivially change solution properties, particularly for the short-chain oligomers, and those changes have been of specific interest.[8]

Here, we analyze the X = CH_3 case. With this capping choice, neutron scattering experiments also characterize C−C contacts for C atoms closer along the chain contour than the end caps, that is, short-circuited loops contribute to those neutron scattering results. In that case, practical chain deuteration avoids the important chemical difficulty, noted above, of specific isotopic labeling of the caps. We utilize simulation results theoretically to investigate anticipated neutron scattering studies that interrogate loop closure. We consider a structure factor model that spans small-angle and diffraction regimes, which thus highlights the molecular-scale features that might be sought.

The structure factor model that we analyze assumes ideal Gaussian chains and is particularly simple. Nevertheless, it is more complicated than the most traditional continuum-Gaussian model, and the distinction is essential for the success of the model in these comparisons.

Special Issue: Branka M. Ladanyi Festschrift

Received: April 30, 2014
Revised: July 16, 2014

 © XXXX American Chemical Society dx.doi.org/10.1021/jp504244x | J. Phys. Chem. B XXXX, XXX, XXX−XXX

We then further test other aspects of Gaussian chain models against simulation results. Because Gaussian chain models are particularly simple, these alternative aspects are typically collective characteristics. Though limited in molecular detail, collective characteristics have countervailing advantages of wide utility. Initial examples include the probability distribution, $P(R_g^2)$, of the square radius of gyration and then the $\langle R_g^2(j)\rangle$ for the jth chain segment, contributing to the decomposition

$$\langle R_g^2\rangle = \frac{1}{n+1}\sum_{j=0}^{n}\langle R_g^2(j)\rangle \tag{1.1}$$

Building from $\langle R_g^2(j)\rangle$ results, we consider density profiles of chain globules described by a Gaussian chain model. Our goal is to establish simple models that permit statistical thermodynamic evaluation of the surface tensions of aqueous electrolyte solutions with hydrocarbon liquids[9−12] when dispersant materials are deployed. As an example of a specific characteristic that should be helpful, we note that the dielectric constant of aqueous PEO solutions depends linearly on the water volume fraction.[7,13]

These systems are notorious for physical complexity despite their chemical simplicity.[14] However, a broad physical description of these solutions is that water is a good solvent for PEO chains, which are swollen by the solvent. Our results for the osmotic second virial coefficients for $CH_3(CH_2{-}O{-}CH_2)_{11}CH_3$, $B_2 > 0$ obtained elsewhere from multichain solution simulations,[7] indicates repulsive *inter*segment interactions at ambient (T,p) conditions. For an experimental perspective on PEG osmotic pressures, see Cohen et al.[15,16] Consistent with repulsive intersegment interactions, we find $\langle R_g^2\rangle \propto m^{1.3}$. Of course, that exponent was not the goal of the calculations implemented, which are detailed below.

Nevertheless, the solution environment sensitively affects PEG conformations.[1,2] PEG molecules are helical in *n*-propanoic, isobutyric, and isopentanoic acid solutions coexisting with liquid water,[2] with helix formation requiring a trace of water.[2] In contrast, these chains are generically coiled in aqueous solutions and also in acetic acid, isobutanol, and *n*-butanol. Conformational sensitivity is associated with size fractionation of PEGs between water and isobutyric acid.[1,2]

The versatility of PEG polymers solutions makes them a challenge for molecular thermodynamics. Flory−Huggins interaction parameters, experimentally evaluated, show substantial but different composition dependences for PEG in water and methanol,[17,18] but in ethanol, there is only minor dependence on composition.[19]

The results below extend the aqueous solution calculations discussed in a preliminary report that compared *n*-hexane solvent with water.[20] Previous simulation calculations[13,21−25] evaluate different aspects of these solutions and give a helpful baseline on which the present modeling builds.

2. METHODS

The simulation calculations below treated a single $CH_3(CH_2{-}O{-}CH_2)_mCH_3$ molecule in water by molecular dynamics, using parallel tempering[26] to achieve enhanced sampling of chain conformations. We evaluated system sizes of $N_{water} = 1000$ (m = 11) and 2000 (m = 21, 31). The chain molecules were represented by optimized potentials for liquid simulations (OPLS-AA),[27] and the SPC/E model was adopted for water[28] implemented with the GROMACS 4.5.3 molecular dynamics simulation package.[29] Long-range electrostatic interactions were treated in standard periodic boundary conditions using particle mesh Ewald with a cutoff of 0.9 nm. The Nosé−Hoover thermostat maintained the temperature, and hydrogen atom bond lengths were constrained by the LINCS algorithm. After energy minimization, density equilibration with (T = 300 K, p = 1 atm) molecular dynamics calculations established the constant volumes for each parallel tempering simulation. The parallel tempering spanned the 256−550 K temperature range with 32 replicas (for m = 11 and 21 cases) and 40 replicas (for m = 31). Parallel tempering swaps were attempted at a rate of 100/ns, and the temperature grid resulted in a success rates of 15−25%. Production calculations for each replica set were extended to 10 ns.

3. RESULTS AND DISCUSSION

The structure factor

$$\frac{\langle|\delta\hat{\rho}_C(k)|^2\rangle}{n_C} = 1 + \int\left(\frac{\sin kr}{kr}\right)\langle\rho_C(r)|0\rangle\,\mathrm{d}\mathbf{r} \tag{3.2}$$

addresses CC loop closure contacts comprehensively, in contrast to chain-end closure exclusively, which would be targeted by labeled ends.[6] Here, n_C is the number of C atoms in the solution, and $\langle\rho_C(r)|0\rangle$ is the density, conditional on placement of a C atom at the origin, of other C atoms at radius r. Because our calculations here treat only one chain molecule, $\langle\rho_C(r)|0\rangle$ is the density of other, *intra*molecular C atoms and is normalized to one less than the number of C atoms in a solute chain; in our case

$$\frac{\langle|\delta\hat{\rho}_C(0)|^2\rangle}{n_C} = 2(m+1) \tag{3.3}$$

The inverse to eq 3.2 is

$$\left(\frac{1}{2\pi}\right)^3\int\left(\frac{\sin kr}{kr}\right)\left(\frac{\langle|\delta\hat{\rho}_C(k)|^2\rangle}{n_C}\right)\mathrm{d}\mathbf{k} = \delta(\mathbf{r}) + \langle\rho_C(r)|0\rangle \tag{3.4}$$

The simple result

$$\frac{\langle|\delta\hat{\rho}_C(k)|^2\rangle}{n_C} = (2m+1)\times[\exp(-k^2\langle R_g^2\rangle) - 1 + k^2\langle R_g^2\rangle]\times\frac{2}{(k^2\langle R_g^2\rangle)^2} \tag{3.5}$$

is the continuum-Gaussian model that we consider.[30] This satisfies the anticipated low-k behavior but not the $k\to\infty$ value associated with the $\delta(\mathbf{r})$ function of eq 3.4. The result for a discrete-Gaussian chain is

$$\left[\frac{\langle|\delta\hat{\rho}_C(k)|^2\rangle}{n_C}\right]_{DG} = \frac{[e^{2\zeta/n}(n+1) - 2(e^{\zeta/n} - e^{-\zeta}) - (n+1)]}{[(n+1)(e^{\zeta/n}-1)^2]} \tag{3.6}$$

where $\zeta = k^2\langle R_g^2\rangle$ and n is the number of Gaussian links. This has the expected $\zeta\to 0$ limit, namely, $(n+1)$ (eq 3.3). Then, $n\to\infty$, with ζ fixed, leads to eq 3.5 and clarifies "continuum" here.

We shift and scale the discrete-Gaussian model

dx.doi.org/10.1021/jp504244x | J. Phys. Chem. B XXXX, XXX, XXX−XXX

$$\frac{\langle |\delta\hat{\rho}_C(k)|^2\rangle}{n_C} - 1 = \left(\frac{2m+1}{n}\right)\left\{\left[\frac{\langle |\delta\hat{\rho}_C(k)|^2\rangle}{n_C}\right]_{DG} - 1\right\} \tag{3.7}$$

to compare with the simulation data (Figure 1). The discrete-Gaussian model matches the data through the low-k regime more

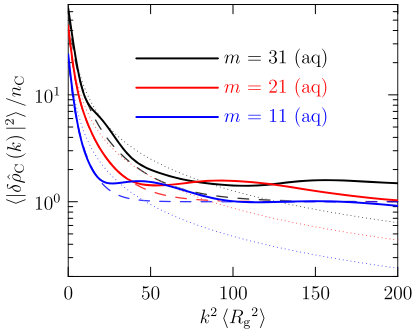

Figure 1. Traditional continuum-Gaussian structure factor (eq 3.5, dotted curves) contrasted with a discrete-Gaussian model, shifted and scaled, which is consistent with the correct $k \to \infty$ limit (eq 3.7, dashed curves). The direct numerical simulation results are the solid curves. For the model of eq 3.7, the number of Gaussian links, n, was adjusted for agreement throughout a low-k regime. In all cases, here, n was about a third of the number of heavy atoms of $CH_3(CH_2{-}O{-}CH_2)_mCH_3$, that is, in coarse-grained models of these oligomers, coarsened monomers can represent about three effective atoms for this characteristic. The local maxima for $k > 0$ here correspond to $k \gtrsim 2\pi/0.6$ nm.

effectively than does the continuum model eq 3.5. Beyond that low-k regime, the data deviate from the discrete-Gaussian model positively through a local maximum, indicating a short length scale $2\pi/k_{max} \lesssim 0.6$ nm.

We can directly turn to $\langle\rho_C(r)|0\rangle$ for confirmation of this inference (Figure 2). Indeed, the short-distance regime begins with $r < 0.6$ nm, consistent with identification of high angles for $k > 2\pi/0.6$ nm (Figure 1).

In addition to the assumption of ideal behavior for the n coarsened monomers, the model tested above obviously utilizes an empirical $\langle R_g^2\rangle$. We next consider the distribution of R_g^2 for these chains, compared to Gaussian model results (Figure 3). The distinctions deriving from molecular-scale resolution, cutoffs at minimum and maximum lengths, are prominent.

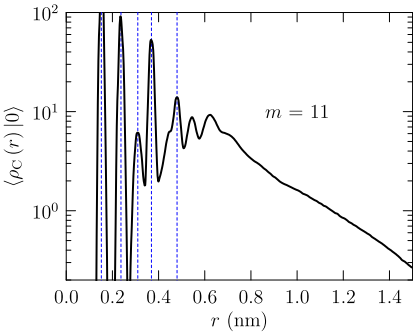

Figure 2. Density, conditional on placement of a C atom at the origin, of other C atoms at radius r; see the text. Consistent with Figure 1, the short-distance regime begins with $r < 0.6$ nm (high angles for $k > 2\pi/0.6$ nm). The dashed vertical lines indicate distances of specific interest. The $r \approx 0.38$ nm peak includes nonbonded CC contacts that are of interest to investigations of hydrophobic interactions.[6]

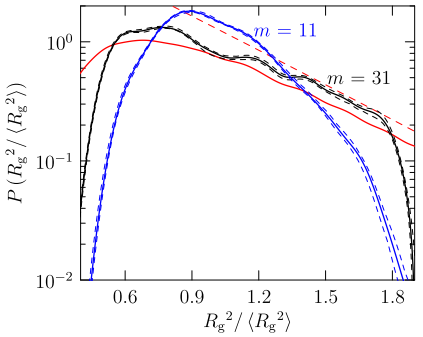

Figure 3. The solid red curve is the result for the $m = 31$ case of a freely jointed chain, obtained numerically by a straightforward Monte Carlo calculation; the dashed red curve is the asymptotic $R_g^2/\langle R_g^2\rangle \approx \infty$ result for an ideal Gaussian model,[31] close to a simple Gaussian function. The dashed lines bracket the 95% confidence intervals approximated by a bootstrap method.

The comparison (Figure 4) of the observed dependence of $\langle R_g^2(j)\rangle$ on contour index j with that for ideal Gaussian models

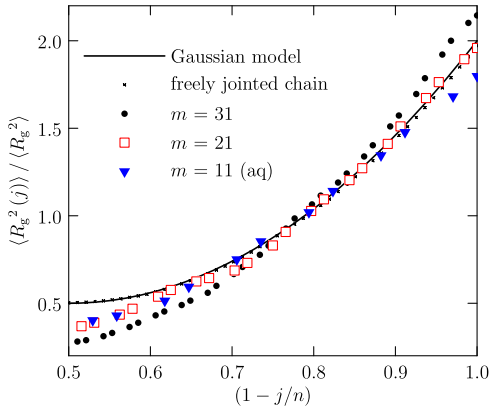

Figure 4. The number of bonds along the heavy atom chain contour is indexed by n, that is, $n = 34$, which has 35 heavy atoms for the $m = 11$ chain. The chain molecule length index m is defined on the basis of the molecular formula $CH_3(CH_2{-}O{-}CH_2)_mCH_3$. The solid curve is the function $2[1 - 3(j/n)(1 - j/n)]$, appropriate for an ideal Gaussian chain.[32] The crosses are the results for the $m = 31$ case of a freely jointed chain, obtained numerically by a straightforward Monte Carlo calculation. The right-most triangle corresponds to a methyl C atom, here with index $j = 34$; $j = 0$ is chemically equivalent. The third triangle from the right boundary corresponds to $j = 31$, chemically equivalent to $j = 3$.

shows encouraging agreement. On the other hand, the discrepancies of ideal Gaussian behavior from the observed results are much larger than the difference of the ideal Gaussian model from the results for a freely jointed chain. Because eq 1.1 is a sum of positive contributions, the ratio plotted in Figure 4 is normalized, and therefore, the behavior seen in Figure 4 expresses the swelling of these chains in water. Thus, it is clear that the quantitative discrepancies are significant, though these characteristics offer minimal expression of molecular detail.

Identifying chemically distinct C atoms permits a layered display of density profiles (Figure 5). C atoms near the center of the chain are likely in the interior of the chain droplet, and the end atoms are more likely on the outside.

The natural comparative model for the density profiles (Figure 6) is obtained by superposing of the Gaussian distributions associated with the observed $\langle R_g^2(j)\rangle$[32]

dx.doi.org/10.1021/jp504244x | J. Phys. Chem. B XXXX, XXX, XXX−XXX

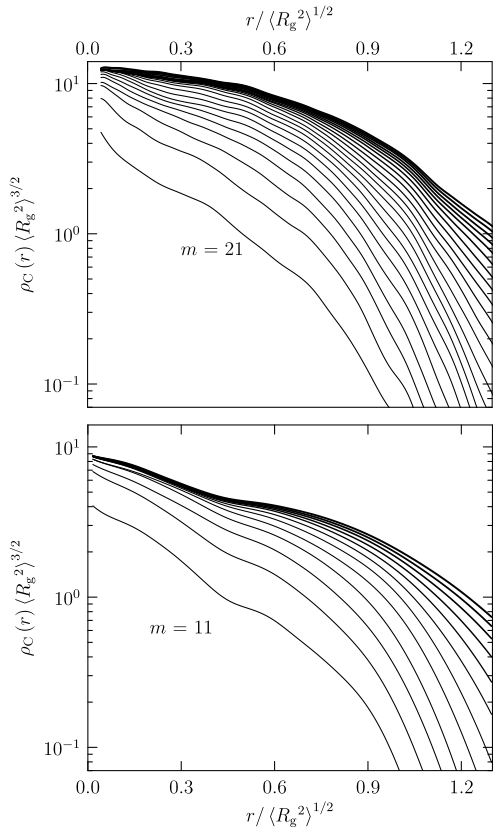

Figure 5. C atom contributions to the chain density profiles from their center of mass, cumulatively indexed by the contour distance from the chain center. The lowest curve corresponds to the midpair C atoms, the next higher curve includes two additional C atoms, and the uppermost curve includes all C atoms.

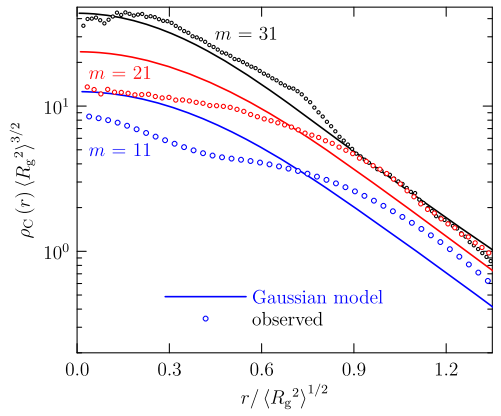

Figure 6. Density profiles for C atoms, relative to their center of mass. The Gaussian models (solid curves) follow from the discussion of Yamakawa,[32] using the empirical $\langle R_g^2(j)\rangle$ shown in Figure 3.

$$\rho_C(r) = \sum_{j=\text{C atoms}} \frac{e^{-3r^2/2\langle R_g^2(j)\rangle}}{\sqrt[3]{2\pi\langle R_g^2(j)\rangle/3}} \tag{3.8}$$

For the $m = 11$ chains, some molecular-scale structure is evident, but that is less prominent (Figure 5) for $m = 21$ chains

4. CONCLUSIONS

Chain structure factors, relevant to neutron scattering from a chain in null water, are compared in detail to a traditional continuum-Gaussian model result. The most serious limitation of the traditional continuum-Gaussian structure factor is the failure to match the trivially known $k \to \infty$ limiting value. A discrete-Gaussian model that is consistent with the correct $k \to \infty$ value is considered. Shifting and scaling of the discrete-Gaussian model helps to identify the low-k to high-k transition near $k \approx 2\pi/0.6$ nm when an empirically matched number of Gaussian links is about one-third of the total number of effective-atom sites. The shifted and scaled discrete-Gaussian model better identifies the transition from low-k to high-k behavior near $k \approx 2\pi/0.6$ nm, which thus provides a natural spatial size for the coarsened monomers. This short distance scale boundary of 0.6 nm is directly verified with the r space distributions.

Further testing of Gaussian chain models for these systems shows that $\langle R_g^2(j)\rangle$, the contribution of the jth chain segment to $\langle R_g^2\rangle$, depends on the contour index about as expected for Gaussian chains despite quantitative discrepancies. The quantitative comparison expresses the swelling of these chains in water. Monomers central to the chain contour are usually central to the chain globule. The density profiles of chain molecule segments relative to their center of mass can show distinctive density structuring for smaller chains due to the close proximity of central elements to the globule center. That density structuring washes out for longer chains, and due to the coarsened length scale $\langle R_g^2\rangle^{1/2}$, many chain elements then contribute additively to the density profiles. Gaussian chain models thus become more satisfactory for the density profiles for longer chains.

AUTHOR INFORMATION

Notes

The authors declare no competing financial interest.

ACKNOWLEDGMENTS

The financial support of the Gulf of Mexico Research Initiative (Consortium for Ocean Leadership Grant SA 12-05/GoMRI-002) is gratefully acknowledged.

REFERENCES

(1) Alessi, M. L.; Norman, A. I.; Knowlton, S. E.; Ho, D. L.; Greer, S. C. Helical and Coil Conformations of Poly(ethylene glycol) in Isobutyric Acid and Water. *Macromolecules* **2005**, *38*, 9333−9340.

(2) Norman, A. I.; Fei, Y.; Ho, D. L.; Greer, S. C. Folding and Unfolding of Polymer Helices in Solution. *Macromolecules* **2007**, *40*, 2559−2567.

(3) *Understanding Oil Spill Dispersants: Efficacy and Effects*; National Academies Press: Washington, DC, 2005.

(4) Lin, Z.; Rubtsov, I. V. Constant-Speed Vibrational Signaling along Polyethyleneglycol Chain up to 60-A Distance. *Proc. Natl. Acad. Sci. U.S.A.* **2012**, *109*, 1413−1418.

(5) Weikl, T. R. Loop-Closure Principles in Protein Folding. *Arch. Biochem. Biophys.* **2008**, *469*, 67−75.

(6) Chaudhari, M. I.; Pratt, L. R.; Paulaitis, M. E. Direct Observation of a Hydrophobic Bond in Loop Closure of a Capped $(-OCH_2CH_2-)_n$ Oligomer in Water. *J. Chem. Phys.* **2010**, *133*, 231102.

(7) Chaudhari, M. I. Molecular Simulations to Study Thermodynamics of Polyethylene Oxide Solutions. Ph.D. Thesis, Department of Chemical & Biomolecular Engineering, Tulane University, 2013.

(8) Dormidontova, E. E. Influence of End Groups on Phase Behavior and Properties of PEO in Aqueous Solutions. *Macromolecules* **2004**, *37*, 7747−7761.

(9) Nichols, A. L.; Pratt, L. R. Disentanglement of Hydrophobic and Electrostatic Contributions to the Film Pressures of Ionic Surfactants. *Faraday Symp. Chem. Soc.* **1982**, *17*, 129−140.

(10) Wilson, M. A.; Nichols, A. L., III; Pratt, L. R. Hydrophobic Interaction of Amphiphilic Ions with Water−Hydrocarbon Liquid Interfaces. *J. Chem. Educ.* **1984**, *81*, 579−580.
(11) Nichols, A. L., III; Pratt, L. R. Salt Effects on the Surface Tensions of Dilute Electrolyte Solutions: The Influence of Nonzero Relative Solubility of the Salt between the Coexisting Phases. *J. Chem. Phys.* **1984**, *80*, 6225−6233.
(12) Pratt, L. R. Contact Potentials of Solution Interfaces: Phase Equilibrium and Interfacial Electric Fields. *J. Phys. Chem.* **1992**, *96*, 25−33.
(13) Borodin, O.; Bedrov, D.; Smith, G. D. Molecular Dynamics Simulation Study of Dielectric Relaxation in Aqueous Poly(ethylene oxide) Solutions. *Macromolecules* **2002**, *35*, 2410−2412.
(14) Israelachvili, J. The Different Faces of Poly(ethyleneglycol). *Proc. Natl. Acad. Sci. USA* **1997**, *94*, 8378−8379.
(15) Cohen, J. A.; Podgornik, R.; Hansen, P. L.; Parsegian, V. A. A Phenomenological One-Parameter Equation of State for Osmotic Pressures of PEG and Other Neutral Flexible Polymers in Good Solvents. *J. Phys. Chem. B* **2009**, *113*, 3709−3714.
(16) Cohen, J. A.; Podgornik, R.; Parsegian, V. A. Finite Length Effects for Osmotic Pressures of PEG Polymers. *Biophys. J.* **2012**, *102*, 400A−400A.
(17) Bae, Y. C.; Shim, D. S.; Soane, J. J.; Prausnitz, J. M. Representation of Vapor−Liquid and Liquid−Liquid Equilibria for Binary Systems Containing Polymers: Applicability of an Extended Flory−Huggins Equation. *J. Appl. Polym. Sci.* **1993**, *47*, 1193−1206.
(18) Zafarani-Moattar, M. T.; Tohidifar, N. Vapor−Liquid Equilibria, Density, and Speed of Sound for the System Poly(ethylene glycol) 400 + Methanol at Different Temperatures. *J. Chem. Eng. Data* **2006**, *51*, 1769−1774.
(19) Zafarani-Moattar, M. T.; Tohidifar, N. Vapor−Liquid Equilibria, Density, Speed of Sound, and Viscosity for the System Poly(ethylene glycol) 400 + Ethanol at Different Temperatures. *J. Chem. Eng. Data* **2008**, *53*, 785−793.
(20) Chaudhari, M. I.; Pratt, L. R. In *Oil Spill Remediation: Colloid Chemistry-Based Principles and Solutions*; Somasundaran, P., Farinato, R., Patra, P., Papadopoulos, K. D., Eds.; John Wiley and Sons, Inc.: New York, 2012; see also arXiv:1208.0349v2.
(21) Borodin, O.; Bedrov, D.; Smith, G. D. A Molecular Dynamics Simulation Study of Polymer Dynamics in Aqueous Poly(ethylene oxide) Solutions. *Macromolecules* **2001**, *34*, 5687−5693.
(22) Lee, H.; Venable, R. M.; MacKerell, A. D., Jr.; Pastor, R. W. Molecular Dynamics Studies of Polyethylene Oxide and Polyethylene Glycol: Hydrodynamic Radius and Shape Anisotropy. *Biophys. J.* **2008**, *95*, 1590−1599.
(23) Choi, E.; Mondal, J.; Yethiraj, A. Coarse-Grained Models for Aqueous Polyethylene Glycol Solutions. *J. Phys. Chem. B* **2013**, *118*, 323−329.
(24) Mondal, J.; Choi, E.; Yethiraj, A. Atomistic Simulations of Poly(ethylene oxide) in Water and an Ionic Liquid at Room Temperature. *Macromolecules* **2014**, *47*, 438−446.
(25) Starovoytov, O. N.; Borodin, O.; Bedrov, D.; Smith, G. D. Development of a Polarizable Force Field for Molecular Dynamics Simulations of Poly (Ethylene Oxide) in Aqueous Solution. *J. Chem. Theory Comput.* **2011**, *7*, 1902−1915.
(26) Earl, D. J.; Deem, M. W. Parallel Tempering: Theory, Applications, and New Perspectives. *Phys. Chem. Chem. Phys.* **2005**, *7*, 3910−3916.
(27) Jorgensen, W. L.; Maxwell, D. S.; Tirado-Rives, J. Development and Testing of the OPLS All-Atom Force Field on Conformational Energetics and Properties of Organic Liquids. *J. Am. Chem. Soc.* **1996**, *118*, 11225−11236.
(28) Berendsen, H. J. C.; Grigera, J. R.; Straatsma, T. P. The Missing Term in Effective Pair Potentials. *J. Phys. Chem.* **1987**, *91*, 6269−6271.
(29) van der Spoel, D.; Lindahl, E.; Hess, B.; Groenhof, G.; Mark, A. E.; Berendsen, H. J. C. GROMACS: Fast, Flexible, and Free. *J. Comput. Chem.* **2005**, *26*, 1701−1718.
(30) Berne, B. J.; Pecora, R. *Dynamic Light Scattering*; John Wiley & Sons: New York, 1976.
(31) Yamakawa, H. *Modern Theory of Polymer Solutions*; Harper & Row: New York, 1971; eq 8.50.
(32) Yamakawa, H. *Modern Theory of Polymer Solutions*; Harper & Row: New York, 1971; Sec. 7a.